40-GHz Active Interferometric Imaging with Noise Transmitters

Stavros Vakalis[#1], Liang Gong[*#2], John Papapolymerou[#3], and Jeffrey A. Nanzer [#4]
[#]Electrical and Computer Engineering, Michigan State University, USA
[*]Electrical Engineering and Telecommunications, University of New South Wales, Australia
{[1]vakaliss, [2]gonglian, [3]jpapapol, [4]nanzer}@msu.edu,

***Abstract* — We present the first active millimeter-wave interferometric imaging system operating at 40 GHz and employing spatial frequency sampling, in a similar fashion with radio astronomy and passive millimeter-wave imaging. Using incoherent noise illumination from multiple transmitters, the sensitivity requirement on the receivers is significantly relaxed compared to passive interferometric imaging systems, reducing the cost and simplifying the hardware. We present the system topology and measurement results for two-dimensional image reconstruction of reflective targets. Three baseband noise sources are upconverted to 40 GHz for the transmitters, and two receivers are used to synthesize an inverse T-array. The inverse T-shaped two-dimensional array boasts 99.6% sparsity compared to a two-dimensional filled aperture. Reflective spheres are used in order to demonstrate the feasibility of this imaging method.**

***Keywords* — Distributed arrays, interferometric imaging, millimeter-wave imaging, noise radar.**

I. Introduction

Microwave and millimeter-wave imaging systems have found a wide spectrum of applications in remote sensing [1], security sensing [2], [3], and medical imaging [4], [5], among other applications. Implementation of such imagers in the millimeter-wave band offers improved resolution compared to those in the microwave region [6], while maintaining good penetration through fog, clouds, smoke, and clothing compared to optical and infrared imagers. Among the various techniques of microwave and millimeter-wave imaging, staring techniques which lack the need for mechanical or electrical scanning, and therefore show potential for fast imaging, have attracted a lot of interest. The recently introduced compressive imagers achieve image reconstruction with fewer samples than traditional imaging systems, but are still limited by their heavy computational load, and their poor tolerance in low signal-to-noise ratio (SNR) [7]. Passive interferometric imagers capture the extremely low power thermal radiation and reconstruct the image capturing samples in the spatial frequency domain [8]. First developed in radio astronomy [9], spatial frequency sampling enables the generation of images using sparse antenna arrays in a staring configuration. In comparison with fully filled multi-element phased arrays that collect samples in the spatial domain, a sparse array necessitates significantly fewer physical elements, reducing the cost and weight significantly.

Spatial frequency sampling relies on pairwise cross-correlations between a small set of antenna elements to reconstruct the image. In similar fashion with a digital camera, it produces images without beam scanning or any mechanical moving parts. Since there is no direct mapping between each pixel and receiver, post-processed images degrade gracefully with element failure, which increases the overall reliability and lifetime of the system. To employ the spatial frequency image reconstruction method, the radiation from the scene must be incoherent in both space and time. Passive interferometric imagers have evidenced the feasibility of detection of human presence out of the incoherent thermal emissions of the human body [10]. Nonetheless, they require highly sensitive receivers with wide bandwidth, which are costly and challenging to design and calibrate, in order to detect the extremely low-power thermal emissions.

In this paper, we introduce the first active spatial frequency sampling imager in the millimeter-wave band and present the image reconstructions from an inverted T-shaped receiving array. By illuminating the scene with noise transmitters, separated at a large number of wavelengths, the reflected radiation is both spatially and temporally incoherent, meeting the condition of the spatial frequency image reconstruction and alleviating the high sensitivity requirement. Measurements were conducted in a semi-enclosed arch range with two conductive spheres. Because of the smaller antenna elements and baselines, compared to microwave frequencies, there is more freedom for designing compact systems. For this two-dimensional system, the aperture area is reduced by 99.6% compared to a fully populated array.

II. Active Incoherent Spatial Frequency Sampling

Any two-dimensional image can be represented by a superposition of an infinite series of spatial sinusoidally-varying signals of different spatial frequencies. In a spatial frequency sampling array, each antenna pair separated by a certain number of wavelengths serves as a correlation receiver and measures the signal at the corresponding spatial frequency. For a given antenna pair with a baseline of D, the received signals for each antenna can be given by

$$V_1(t) = \cos(2\pi f t) + n_1(t) \tag{1}$$

$$V_2(t) = \cos[2\pi f(t-\tau_g)] + n_2(t) \tag{2}$$

where f is the carrier frequency, n_i is the noise that the i^{th} element receives, and $\tau_g = \frac{D}{c}\sin\theta$ is the geometric

time delay in which c is the speed of light and θ is the azimuth angle between the baseline D and the point source. The two received signals are cross-correlated (multiplied and integrated), and because the signal voltage is incoherent with the noise components and the noise components are incoherent with each other, the noise components will average to zero as integration time increases. The response of the correlation interferometer can be given by

$$r(\theta) = \langle V_1 V_2 \rangle = \langle \cos(2\pi f t) \cos[2\pi f (t - \tau_g)] \rangle. \quad (3)$$

Using a low-pass filter will cut off the high carrier frequency terms, resulting in

$$r(\theta) = \frac{1}{2} \cos\left(\frac{2\pi}{\lambda} D \sin\theta\right) \quad (4)$$

where $\lambda = c/f$ is the corresponding wavelength. The result is a fringe response with a number of sidelobes equal to the corresponding spatial frequency D/λ. However in order for this process to work, as dictated by the Van-Cittert Zernike theorem, the received radiation must be spatio-temporally incoherent [11].

Consider an antenna baseline in the interferometric array observing two point sources as shown in Fig. 1, where the two receiver voltages can be expressed as [12]:

$$V_1 = s_{1A} + s_{1B} + n_1 \quad (5)$$

$$V_2 = s_{2A} + s_{2B} + n_2 \quad (6)$$

where s_{iA}, s_{iB} are the terms that represent the response on the i^{th} element due to the point sources A and B respectively, and n_i is the noise received by the i^{th} element. The output voltage, after cross-correlating the two receiver responses, can by given by:

$$\begin{aligned} V_{out} &= \langle V_1 V_2 \rangle \\ &= \langle s_{1A} s_{2A} \rangle + \langle s_{1B} s_{2B} \rangle + \langle s_{1A} s_{2B} \rangle + \langle s_{1B} s_{2A} \rangle \end{aligned} \quad (7)$$

Using a traditional pulsed radar system to illuminate the scene will result in large correlation between the self and the cross product terms. By illuminating the scene in a spatio-temporally incoherent fashion, the signals from the point sources have very low correlation with each other, they are uncorrelated with the noise components, and the noise components are uncorrelated with each other. The output voltage of the correlation interferometer can be written as:

$$V_{out} = \langle V_1 V_2 \rangle = \langle s_{1A} s_{2A} \rangle + \langle s_{1B} s_{2B} \rangle \quad (8)$$

where $\langle s_{1A} s_{2A} \rangle$ and $\langle s_{1B} s_{2B} \rangle$ represent the common parts from the two point sources. Eq. 8 does not provide complete information about the two point responses, but in an antenna array with multiple antenna pairs the spatial information can be resolved. However, as we assumed above the received signals from the point sources need to be incoherent with each other and that is why most previous work in interferometric imaging has taken place with passive systems which measure

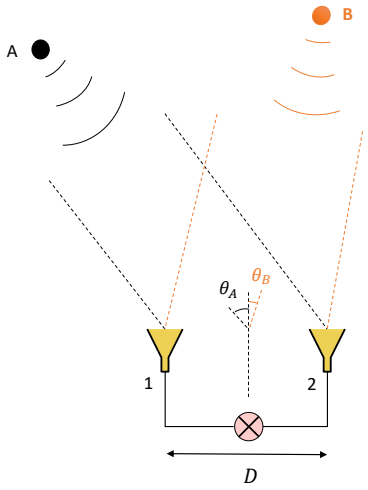

Fig. 1. Two elements of an interferometric array observing two radiating sources.

the thermally generated electromagnetic radiation. Thermal radiation is inherently noise-like, satisfying this requirement.

For this reason, almost all previous work has been with passive systems, because thermal radiation satisfies this requirement [13]. If the radiation intensity of the scene I is spatio-temporally incoherent, then by sampling a large set of the spatial frequency samples of the scene, the sampled visibility V_s is obtained, and the intensity can be reconstructed through an inverse Fourier transform (IFT) by $I_r = IFT\{V_s\}$, where I_r is the reconstructed intensity of the scene.

Prior work has demonstrated that by illuminating a two-dimensional scene with multiple noise transmitters separated by a large number of wavelengths, an incoherent spatio-temporal pattern is created, and as a result, traditional spatial frequency sampling techniques can be used [14]. The signals transmitted from the noise sources are temporally incoherent with each other, and by separating them at a large number of wavelengths, they start interfering in space, mimicking the properties of thermal radiation. Previous work took place in the ISM 5.85 GHz band with an Arbitrary Waveform Generator (AWG) as the noise source. As a result, by operating in a higher signal-to-noise ratio (SNR), bandwidth and integration time was decreased by an order of magnitude or more compared to other published systems. This technique also retains the benefits of interferometric processing, such as staring operation and tolerance to element failures [15]. However, because the system operated at 5.85 GHz, the image resolution was fairly coarse relative to that needed for the applications stated in the introduction.

III. Experimental Setup and Measurement Results

To improve the resolution and achieve a more compact imaging system, the work presented in this paper operates at 40 GHz. The schematic of the experimental configuration can be seen in Fig. 2. The transmitters are three 0.2-2000 MHz low-cost baseband noise sources. For a flatter noise response

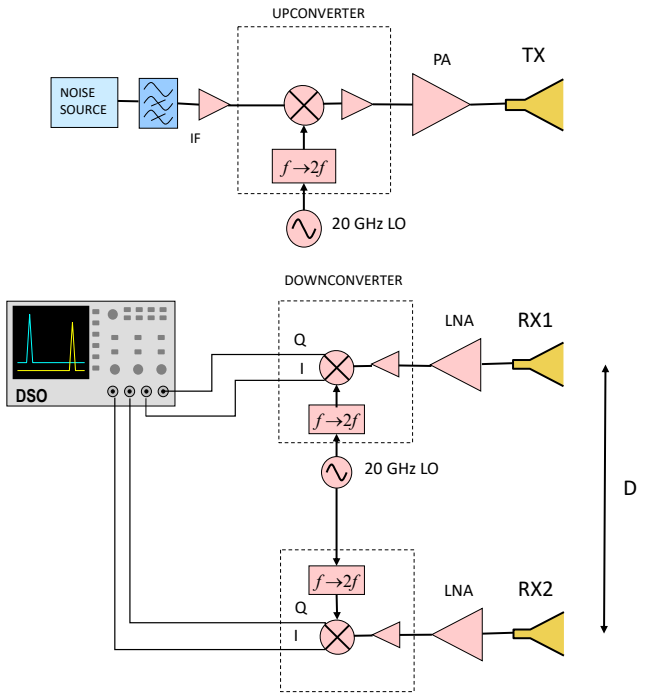

Fig. 2. The schematic of the experimental configuration used in this work. The transmitter consists of three noise sources upconverted to 40 GHz (only one shown in the figure), while the receiver consists of two elements downconverted to baseband and captured using an oscilloscope.

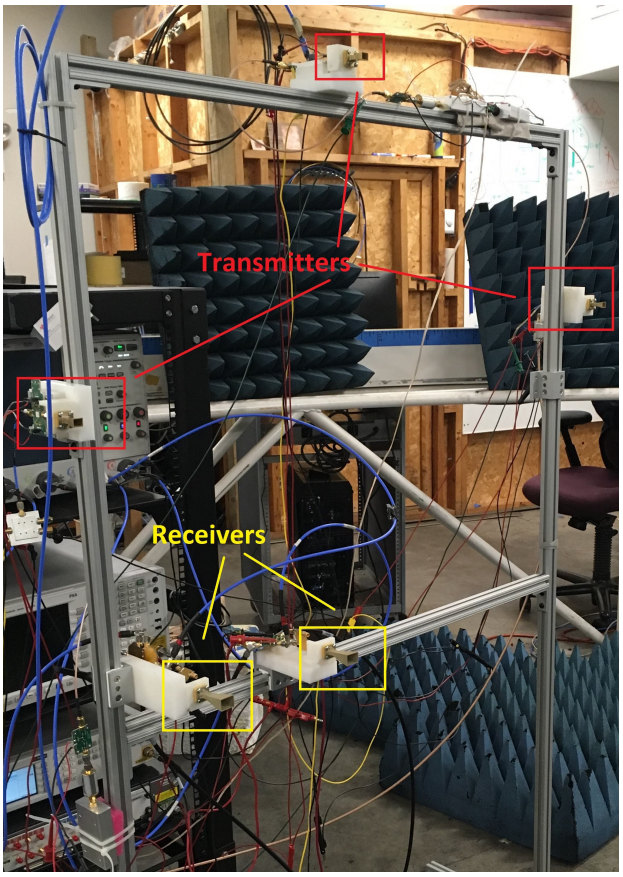

Fig. 3. The rack with all components properly biased and attached. Three noise transmitters were used to illuminate the scene. Two receivers were used to synthesize a two-dimensional array by moving them in the vertical and horizontal directions accordingly.

over the band of interest, a high pass filter with a cutoff frequency of 20 MHz was used after each noise source, followed by a low-cost baseband amplifier of 30 dB gain and subsequently feeding to the IF port of each upconverter. Three GaAs MMIC I/Q upconverters (Analog Devices HMC6787ALC5A), integrated with a frequency doubler for the local oscillator (LO) and a conversion gain of 10 dB, were used to mix the baseband noise to 40 GHz with an LO of 20 GHz. The 40 GHz noise signal was then boosted by three 40 GHz power amplifiers, achieving approximately -10 dBm of noise power at 40 GHz. Each channel is connected to a 10-dBi Ka-band horn antenna.

For the receivers, the reflected noise is received by two 15 dBi horn antennas and amplified with 20 dB gain low-noise amplifiers before being downconverted to baseband using two 37-44 GHz GaAs MMIC I/Q downconverters. All the components were properly biased and fixed into an aluminium rack with 3-D printed holding structures. The rack and all components can be seen in Fig. 3. The downconverted baseband signals were captured and digitized using a 20 GHz oscilloscope in high-resolution mode and processed offline in MATLAB.

Two spherical reflective targets were used as the two-dimensional scene, as shown in Fig. 4. They were placed 2.5 m away from the rack with the smaller one at the center axis of the rack while the bigger one on the left. The horizontal and vertical separation between the spheres was 70 cm and 50 cm, respectively. The synthesized array had a maximum horizontal and vertical dimension of 66λ and 46λ, respectively. The shape of the synthesized array was an inverse T-array in 2λ increments, and the element locations can be seen in Fig. 5. The reconstructed image is shown in Fig. 6. As expected, both the spheres can be clearly resolved and discriminated. The smaller sphere results in a response near the top right of the reconstructed image whereas the bigger sphere shows a larger response on the lower left with higher intensity, as is expected due to its larger radar cross section. There is some sidelobe structure in the image, because of the narrow baselines missing, due to the horn antenna and receiver dimensions, which can be reduced by using smaller antennas and different feeding structures.

IV. Conclusion

The first millimeter-wave active interferometric imager was presented. Using the concept of spatial frequency sampling and illuminating the scene with noise, a cost-effective solution with a sparse array and off-the-shelf components is achieved. Good resolution and the ability of distinguishing reflective targets has been demonstrated by experiment. Compared to other millimeter-wave imaging techniques, the presented approach has the potential for significantly lower cost and

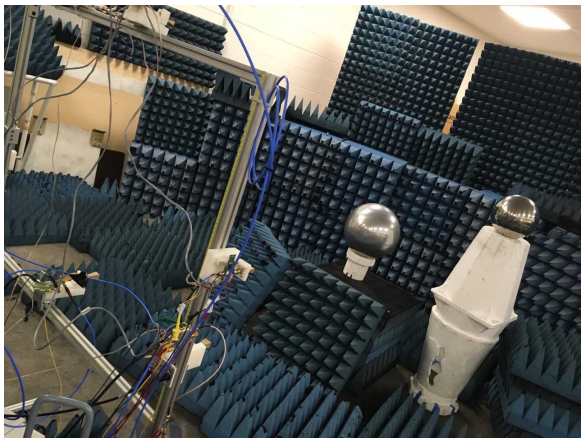

Fig. 4. The two reflective spherical targets placed in the semi-closed anechoic chamber used for the two-dimensional measurements.

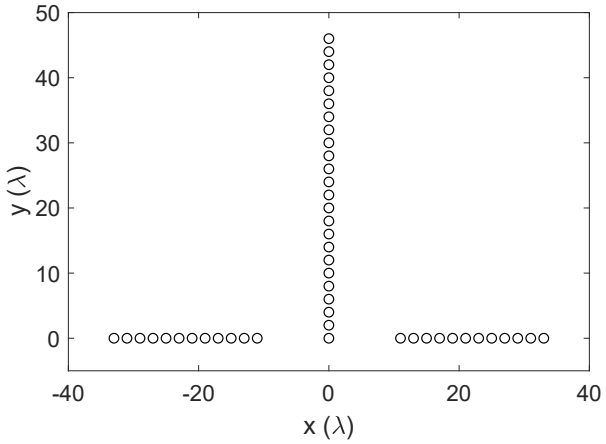

Fig. 5. Element locations for the two-dimensional imaging setup. Two antennas were used and moved sequentially until all antenna pairs were represented in the measurement, in 2λ increments.

better form-factor integration, which may lead to rapid and broad adoption of millimeter-wave imaging in a broad range of applications, including security sensing, remote sensing, vehicular and medical imaging.

V. Acknowledgment

The authors would like to thank Brian Wright, Michigan State University, for help with assembling the experimental setup. This material is based upon work supported by the National Science Foundation under Grant ECCS-1708820.

References

[1] C. T. Swift, D. M. LeVine, and C. S. Ruf, "Aperture synthesis concepts in microwave remote sensing of the earth," *IEEE Transactions on Microwave Theory and Techniques*, vol. 39, no. 12, pp. 1931–1935, Dec 1991.

[2] R. Appleby and R. N. Anderton, "Millimeter-wave and submillimeter-wave imaging for security and surveillance," *Proceedings of the IEEE*, vol. 95, no. 8, pp. 1683–1690, Aug 2007.

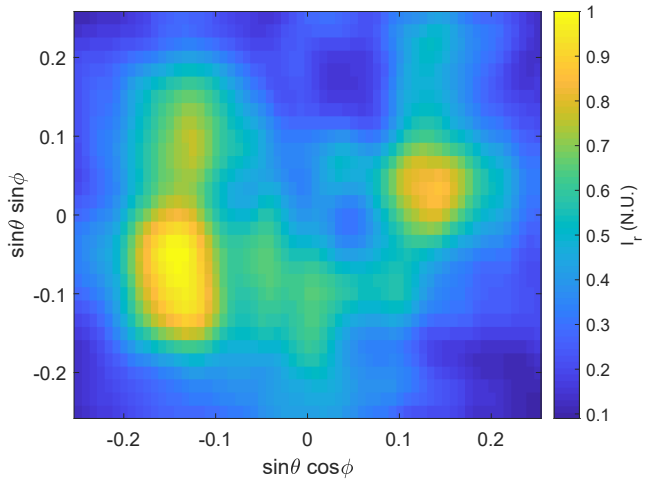

Fig. 6. Experimental image reconstructed intensity (I_r) from two reflective spherical targets. The vertical and horizontal axis are in terms of the direction cosines of the elevation and azimuth planes. The amplitude is normalized, and hence the colorbar axis is in normalized units (N.U.)

[3] D. M. Sheen, D. L. McMakin, and T. E. Hall, "Three-dimensional millimeter-wave imaging for concealed weapon detection," *IEEE Transactions on Microwave Theory and Techniques*, vol. 49, no. 9, pp. 1581–1592, Sep 2001.

[4] N. K. Nikolova, "Microwave imaging for breast cancer," *IEEE Microwave Magazine*, vol. 12, no. 7, pp. 78–94, Dec 2011.

[5] E. J. Bond, X. Li, S. C. Hagness, and B. D. V. Veen, "Microwave imaging via space-time beamforming for early detection of breast cancer," *IEEE Transactions on Antennas and Propagation*, vol. 51, no. 8, pp. 1690–1705, Aug 2003.

[6] Y. Chu, K. Xu, Y. Zhong, X. Ye, T. Zhou, X. Chen, and G. Wang, "Fast microwave through wall imaging method with inhomogeneous background based on levenberg-marquardt algorithm," *IEEE Transactions on Microwave Theory and Techniques*, pp. 1–10, 2018.

[7] J. Hunt, T. Driscoll, A. Mrozack, G. Lipworth, M. Reynolds, D. Brady, and D. R. Smith, "Metamaterial apertures for computational imaging," *Science*, vol. 339, no. 6117, pp. 310–313, 2013.

[8] T. Fromenteze, C. Decroze, S. Abid, and O. Yurduseven, "Sparsity-driven reconstruction technique for microwave/millimeter-wave computational imaging," *Sensors*, vol. 18, no. 5, 2018. [Online]. Available: http://www.mdpi.com/1424-8220/18/5/1536

[9] A. R. Thompson, J. M. Moran, and G. W. Swenson, *Interferometry and Synthesis in Radio Astronomy*. John Wiley and Sons, 2001.

[10] L. Yujiri, M. Shoucri, and P. Moffa, "Passive millimeter wave imaging," *IEEE Microwave Magazine*, vol. 4, no. 3, pp. 39–50, Sept 2003.

[11] M. Born and E. Wolf, *Principles of optics*. Cambridge Univ. Pr., 1999.

[12] J. A. Nanzer, *Microwave and Millimeter-Wave Remote Sensing for Security Applications*. Artech House, 2012.

[13] N. A. Salmon, R. Macpherson, A. Harvey, P. Hall, S. Hayward, P. Wilkinson, and C. Taylor, "First video rate imagery from a 32-channel 22-ghz aperture synthesis passive millimetre wave imager," *Proc. SPIE*, vol. 8188, 2011.

[14] S. Vakalis and J. A. Nanzer, "Microwave imaging using noise signals," *IEEE Transactions on Microwave Theory and Techniques*, pp. 1–10, 2018.

[15] S. Vakalis and J. A. Nanzer, "Analysis of element failures in active incoherent microwave imaging arrays using noise signals," *IEEE Microwave and Wireless Components Letters*, vol. 29, no. 2, pp. 161–163, Feb 2019.